Supplementary Figures

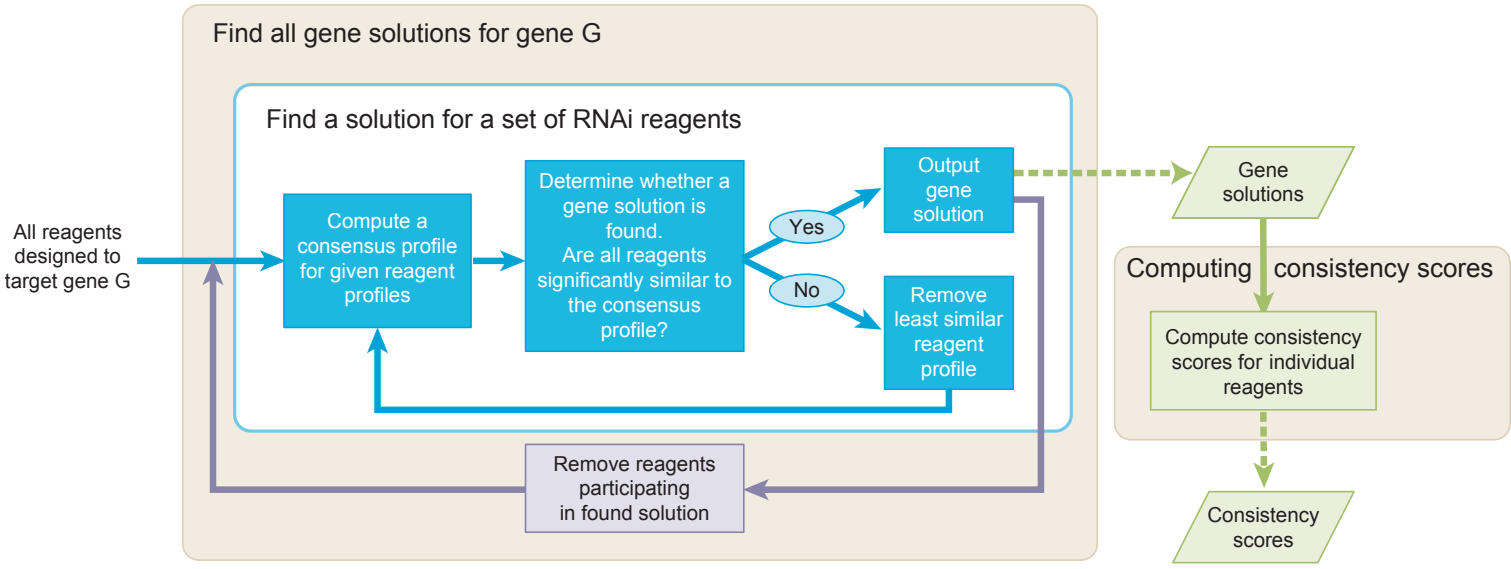

Supplementary Figure 1. A schematic diagram of the ATARiS algorithm.

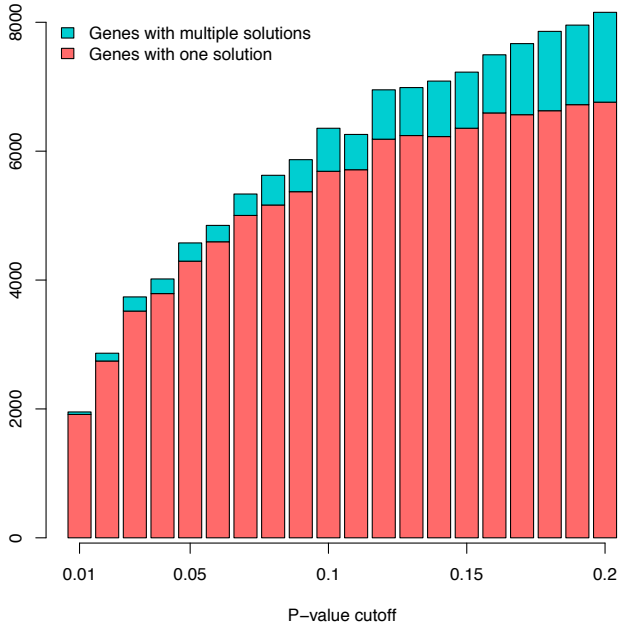

Supplementary Figure 2. Influence of *p*-value cutoff on the number of ATARiS gene solutions. ATARiS was run on the Achilles dataset using p-value cutoffs of 0.01, 0.02, …, 0.20 and the number of genes for which gene solutions were identified is plotted. Each bar represents the median value across 10 ATARiS runs.

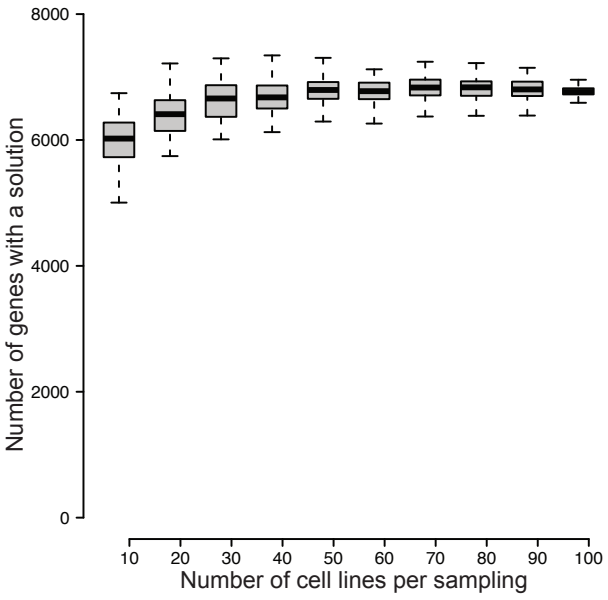

Supplementary Figure 3. Influence of sample size on the number of ATARiS gene solutions. We applied ATARiS to one hundred sets of randomly selected samples (out of the total 102 Achilles Project samples) for each of the indicated sample sizes. The distribution of the number of genes with a solution is shown as a box plot for each sample size.

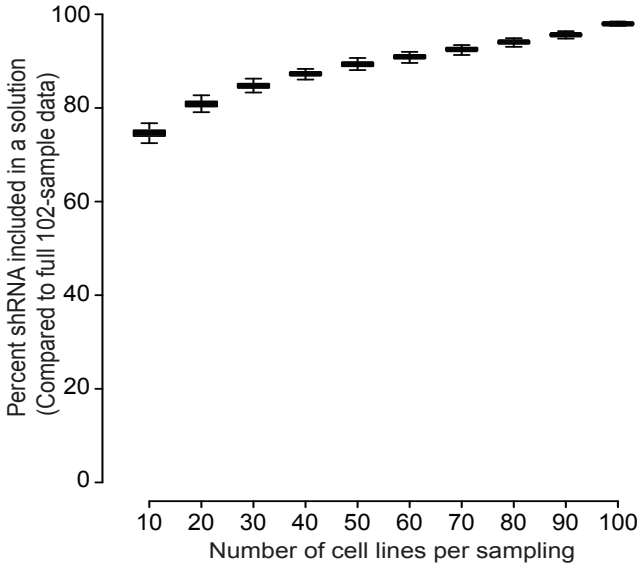

Supplementary Figure 4. Representation of shRNAs in ATARiS solutions after subsampling from the full 102-sample data. We applied ATARiS to one hundred sets of randomly selected samples (out of the total 102 Achilles Project samples) for each of the indicated sample sizes. For each run of subsampled data, we calculated the proportion of shRNAs participating in any gene solution identified in the full 102-sample dataset that are included in a gene solution from the run. Results for each subsample size are displayed as a boxplot.

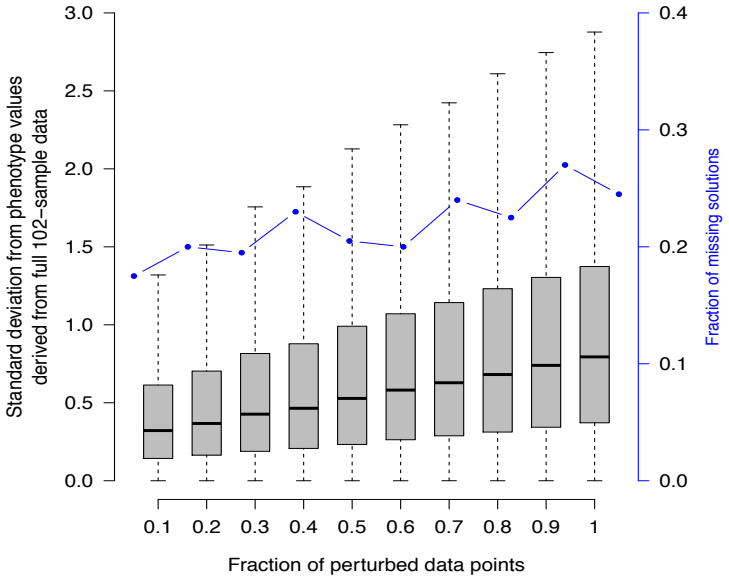

Supplementary Figure 5. Robustness of ATARiS to noise.
We generated perturbed datasets by adding random noise to varying fractions of the original shRNA measurements in the full Achilles dataset (*x* axis). We used a Gaussian noise model with mean zero and variance equal to each shRNA's variance. We compared the results of running ATARiS on the perturbed datasets to the ATARiS results on the full 102-sample Achilles dataset. We randomly selected 100 genes for which a solution was identified in the full Achilles dataset. The boxplots depict the differences between phenotype values computed using the perturbed datasets and the full dataset in standard deviation units (i.e. each unit is the standard deviation of that gene phenotype values across all samples when using the full 102-sample dataset). The figure also shows the fraction of genes (out of the 100) for which a solution was not identified in the perturbed datasets. Results were generated using 10 perturbed datasets for each perturbation level.

a

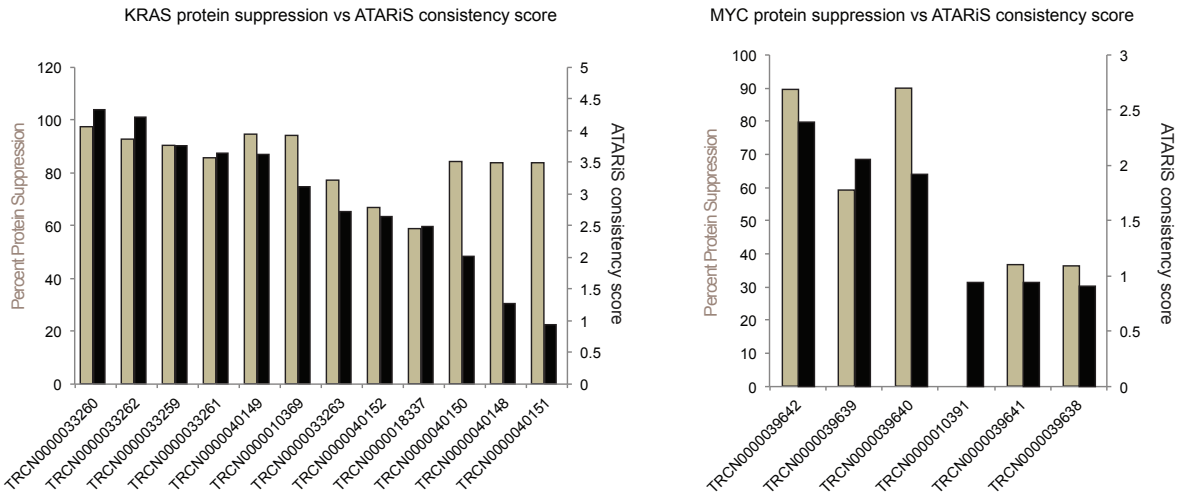

b

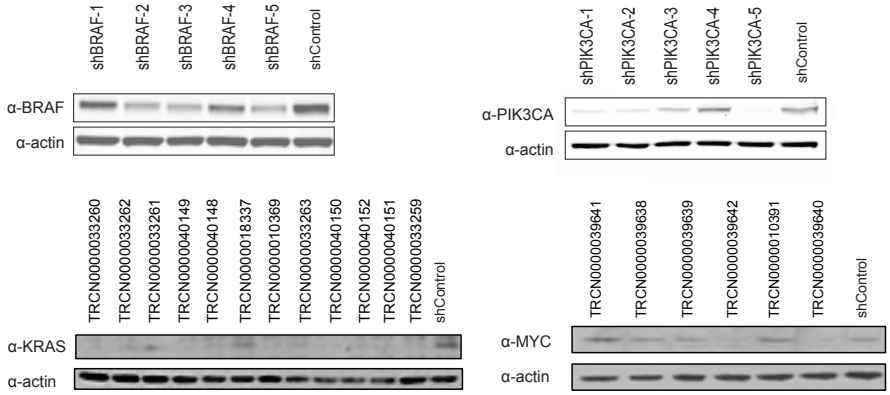

Supplementary Figure 6. Comparison of shRNA consistency score to protein suppression. (a) ATARiS consistency scores for individual shRNAs targeting KRAS or MYC are compared to relative protein suppression of the target protein. Immunoblotting was performed in cell line A549 and percent suppression was calculated after quantification of bands by ImageJ software. Colors on axis labels correspond to data bars of the same color. (**b**) Immunoblots used for quantification of protein suppression as shown in manuscript Figure 3 and panel **a** above.

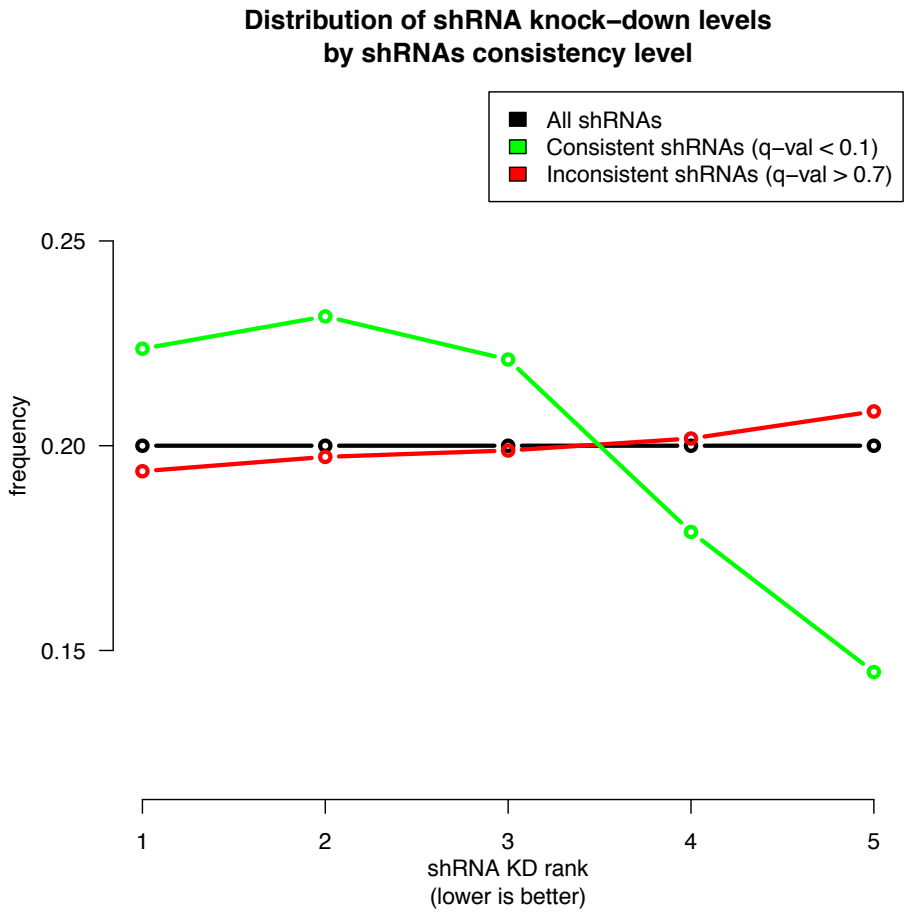

Supplementary Figure 7. On-target gene suppression measured by high-throughput qRT-PCR is associated with higher consistency scores. Using high-throughput qRT-PCR data of shRNAs (manuscript in preparation; data available on request) we analyzed screening data for genes with exactly five shRNAs with high confidence qRT-PCR data (n=9,050 shRNAs). For each gene, we ranked the level of mRNA suppression of each of its shRNAs from 1 to 5 (1, most suppressed; 5, least suppressed), and assessed the frequency of each rank for those shRNAs predicted to perform well by ATARiS (consistency score q-value < 0.1). For comparison, we show the frequency of mRNA ranks when using shRNAs that have low consistency scores (consistency score q-values > 0.7), or all shRNA.

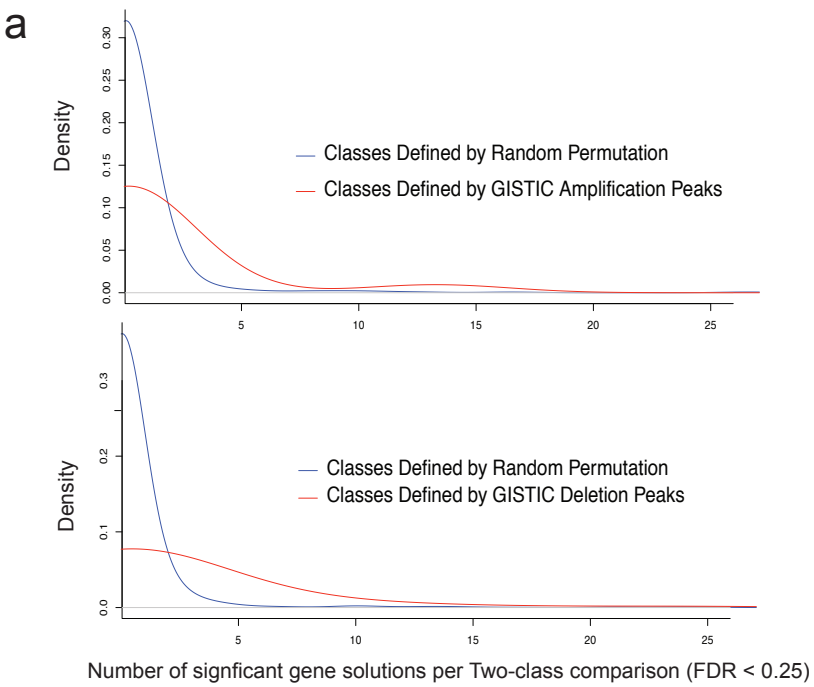

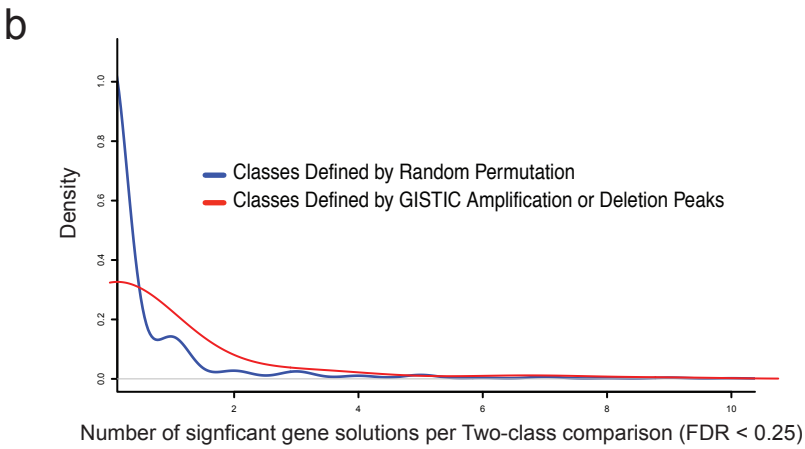

Supplementary Figure 8. Differentially essential gene solutions from two-class comparisons of significant amplification and deletion peaks. Peaks were defined by GISTIC analysis across samples from the Cancer Cell Line Encyclopedia (http://broadinstitute.org/ccle). To determine genes significantly essential in samples harboring each peak, we calculated the difference in means between two classes determined by the presence or absence of each peak. *P*-values were estimated from an empirical null distribution by permutation of peak assignments. Significant genes were defined as those whose False Discovery Rate (FDR) adjusted *p*-value was less than 0.25. For comparison, we show the distribution of significant genes when assigning random peaks to samples. Random peak assignments were made by permutation of the real peak distribution across samples. (a) Results for amplification peaks (above) or deletion peaks (below) using all gene solutions from the Achilles data. (b) Results for combined amplification and deletion peaks after excluding the first ("primary") gene solution found for each gene.

Rank	Phenotype	P.Value	Q.Value
1	Gistic.DelPeak1.1p36.31	0.00105	0.00105
2	Gistic.DelPeak4.1p21.3	0.01040	0.01040
3	Gistic.DelPeak2.1p33	0.01430	0.01430
4	Gistic.DelPeak3.1p31.1	0.02170	0.02170
5	Gistic.AmpPeak29.13q31.3	0.03030	0.03030
6	Gistic.AmpPeak30.13q34	0.03320	0.03320
7	Gistic.DelPeak10.3p14.2	0.03790	0.03790
8	Gistic.DelPeak21.6q26	0.04740	0.04740
9	Mut.CNA.RB1	0.05960	0.05960
10	Gistic.DelPeak15.4q22.1	0.06940	0.06940
11	Lineage.colorectal	0.08270	0.08270
12	Gistic.AmpPeak22.11p13	0.08290	0.08290
13	Gistic.DelPeak23.7q31.1	0.08690	0.08690
14	Gistic.AmpPeak6.2p24.3	0.09320	0.09320
15	Gistic.AmpPeak28.12q14.1	0.12000	0.12000
16	Gistic.DelPeak47.16p13.2	0.12300	0.12300
17	Gistic.DelPeak16.4q35.1	0.12500	0.12500
18	Mut.APC	0.14300	0.14300
19	Lineage.lung_small_cell	0.15500	0.15500
20	Gistic.DelPeak11.3p12.1	0.16200	0.16200

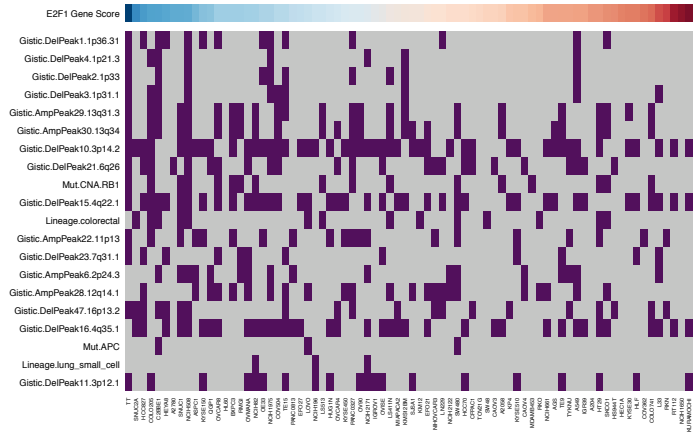

Supplementary Figure 9. Relationship between genomic features and E2F1 phenotype values. Using ATARiS phenotype values for *E2F1* (blue – negative; red – positive), we ranked the annotated genomic features (see Methods for annotation of features) for each sample based on the degree to which presence of each feature corresponds to dependency on *E2F1*. Features were ranked by theoretical *p*-value calculated by Mann-Whitney test for ability to discriminate for samples that are highly dependent on *E2F1*. Gistic, peaks defined by GISTIC algorithm. DelPeak, deletion peak. AmpPeak, amplification peak. Mut.CNA, mutation or copy-number loss. Mut, mutation. Purple, presence of indicated feature. Grey, absence of indicated feature.

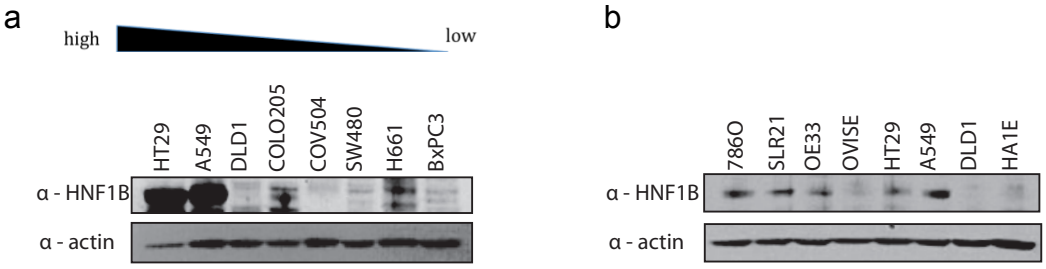

Supplementary Figure 10. HNF1B protein expression level in cancer cell lines. Relationship between HNF1B gene phenotype value and expression in a panel of cell lines ordered from high to low dependence (a). Specific cell lines used in Fig. 6c in the manuscript (b).

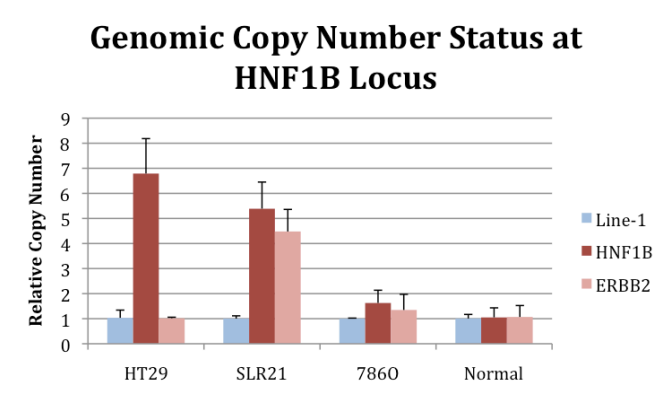

Supplementary Figure 11. Genomic copy number status at the HNF1B locus as assessed by quantitive PCR of genomic DNA. HT29 harbored known amplification of HNF1B. SLR21 and 786O had unknown copy number status but were identified as dependent by ATARiS phenotype values and subsequent validation. Error bars, +/- one standard deviation (*n*=3). Primers complementary to Line-1 genomic repetitive elements were used for normalization, and normal human DNA (Applied Biosystems) was used as reference.

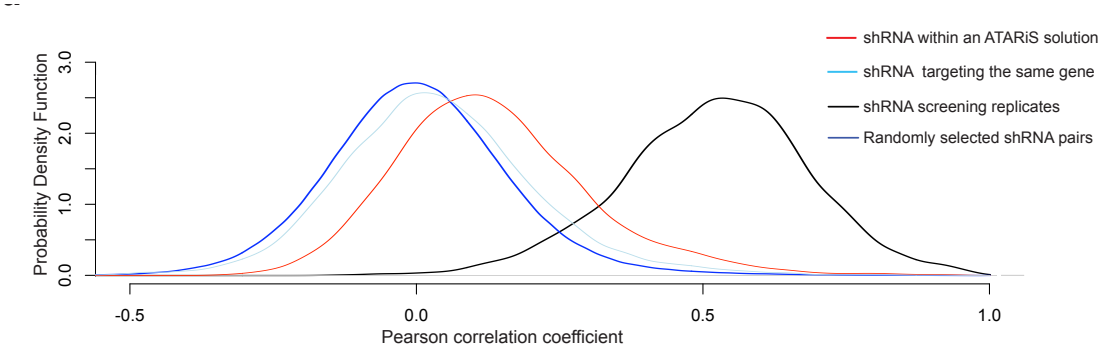

Supplementary Figure 12. Similarity between effects produced by shRNAs across 102 screened samples. ShRNAs targeting 500 randomly selected genes were used to calculate Pearson correlation coefficients for screening data between all pairs of shRNA within each indicated set. Density distributions (Probability Density Function) of the correlation coefficients for each set are displayed in the indicated color. As expected, the correlations between shRNA profiles within ATARiS solutions are significantly higher than those between randomly selected pairs of shRNA profiles (*p*-value < 2.2×10^{-16}, Welch's *t*-test) and were also significantly higher than the correlations between profiles of shRNAs targeting the same gene (*p*-value < 2.2×10^{-16}, Welch's *t*-test), demonstrating that ATARiS identifies shRNAs with consistent effects.

Supplementary Tables

Supplementary Table 1. Results for genes calculated from Achilles RNAi dataset. We account for all genes screened in terms of number of shRNAs used to target that gene and the resulting number of gene solutions identified by ATARiS.

		Number of shRNAs per gene																
		2	**3**	**4**	**5**	**6**	**7**	**8**	**9**	**10**	**11**	**12**	**13**	**14**	**15**	**19**	**20**	**Totals**
Number of gene solutions per gene	**0**	53	256	1041	2577	12	8	0	3	4	1	0	0	0	0	0	0	**3955**
	1	24	230	1346	4549	20	24	14	10	12	2	0	0	1	0	1	0	**6233**
	2	0	0	98	844	5	14	7	9	18	4	3	1	0	2	0	0	**1005**
	3	0	0	0	0	0	0	2	1	5	1	0	0	1	0	0	1	**11**
	4	0	0	0	0	0	0	0	0	0	0	1	0	0	0	0	0	**1**
																		11205

Supplementary Table 2. Rank of dependency phenotype value in two-class comparison by mutation Status for common oncogenes.

Classes	Gene	Rank	P.Val	Q.Val
KRAS Mutation	*KRAS*	1	2.00E-05	0.053
BRAF Mutation	*BRAF*	1	2.00E-05	0.158
PI3Kinase Mutation	*PIK3CA*	1	2.00E-05	0.147

Supplementary Table 3. Results for genes calculated from Marcotte *et al.* dataset. We account for all genes screened in terms of number of shRNAs used to target that gene and the resulting number of gene solutions identified by ATARiS.

		Number of shRNAs per gene																
		2	**3**	**4**	**5**	**6**	**7**	**8**	**9**	**10**	**11**	**12**	**13**	**14**	**15**	**16**	**17+**	**Totals**
Number of gene solutions per gene	**0**	34	136	986	5828	11	13	12	6	7	3	0	2	0	2	0	2	**7042**
	1	11	111	861	5423	4	19	25	1	7	2	2	2	0	0	0	1	**6469**
	2	0	0	88	1752	2	15	17	11	6	0	2	2	0	0	0	5	**1900**
	3	0	0	0	0	0	1	6	4	3	1	4	2	0	0	0	4	**25**
	4	0	0	0	0	0	0	0	0	0	1	2	0	1	0	1	4	**9**
	5+	0	0	0	0	0	0	0	0	0	0	1	0	0	0	0	2	**3**
																		15448

Supplementary Table 4. Identities of 83 Project Achilles cell lines for which expression microarrays are available in the Cancer Cell Line Encyclopedia (http://broadinstitute.org/ccle).

786O_KIDNEY
A204_SOFT_TISSUE
A2058_SKIN
A2780_OVARY
A549_LUNG
AGS_STOMACH
ASPC1_PANCREAS
BXPC3_PANCREAS
C2BBE1_LARGE_INTESTINE
CAOV3_OVARY
CAOV4_OVARY
CFPAC1_PANCREAS
COLO205_LARGE_INTESTINE
COLO741_SKIN
COV362_OVARY
COV434_OVARY
COV504_OVARY
DLD1_LARGE_INTESTINE
EFO21_OVARY
EFO27_OVARY
GP2D_LARGE_INTESTINE
HCC70_BREAST
HCC827_LUNG
HEC1A_ENDOMETRIUM

HEYA8_OVARY
HL60_HAEMATOPOIETIC_AND_LYMPHOID_TISSUE
HLF_LIVER
HS944T_SKIN
HT29_LARGE_INTESTINE
HUG1N_STOMACH
HUTU80_SMALL_INTESTINE
IGR39_SKIN
IGROV1_OVARY
KM12_LARGE_INTESTINE
KMS12BM_HAEMATOPOIETIC_AND_LYMPHOID_TISSUE
KP4_PANCREAS
KURAMOCHI_OVARY
KYSE150_OESOPHAGUS
KYSE30_OESOPHAGUS
KYSE450_OESOPHAGUS
KYSE510_OESOPHAGUS
L33_PANCREAS
LN229_CENTRAL_NERVOUS_SYSTEM
LOVO_LARGE_INTESTINE
LS411N_LARGE_INTESTINE
LS513_LARGE_INTESTINE
MDAMB453_BREAST
MIAPACA2_PANCREAS
NCIH1650_LUNG
NCIH196_LUNG
NCIH1975_LUNG
NCIH2122_LUNG
NCIH2171_LUNG
NCIH508_LARGE_INTESTINE
NCIH661_LUNG
NCIH82_LUNG
NIHOVCAR3_OVARY
OE33_OESOPHAGUS
OV90_OVARY
OVCAR4_OVARY
OVCAR8_OVARY
OVISE_OVARY
OVMANA_OVARY
PANC0327_PANCREAS
PANC0813_PANCREAS
QGP1_PANCREAS
RKN_OVARY
RKO_LARGE_INTESTINE
RMGI_OVARY
RT112_URINARY_TRACT
SJSA1_BONE

SKCO1_LARGE_INTESTINE
SNU840_OVARY
SNUC1_LARGE_INTESTINE
SNUC2A_LARGE_INTESTINE
SW480_LARGE_INTESTINE
SW48_LARGE_INTESTINE
TE15_OESOPHAGUS
TE9_OESOPHAGUS
TOV21G_OVARY
TT_OESOPHAGUS
TYKNU_OVARY
U251MG_CENTRAL_NERVOUS_SYSTEM

Supplementary Table 5. Table of genes that are essential in samples with high expression. Top 75 results are shown. Known cancer drivers are highlighted in red.

Rank	ATARiS Solution	Gene	Correlation	P-Value	FDR
1	HNF1B_1_11000	HNF1B	-0.553	2.00E-05	0.075
1	PAX8_1_10011	PAX8	-0.534	2.00E-05	0.075
3	E2F3_1_11111	E2F3	-0.427	4.00E-05	0.075
3	ELF3_1_01001	ELF3	-0.434	4.00E-05	0.075
5	SOX10_1_01111	SOX10	-0.436	6.00E-05	0.075
5	HIST1H4D_1_0101	HIST1H4D	-0.422	6.00E-05	0.075
7	NGEF_1_01101	NGEF	-0.433	8.00E-05	0.086
8	FERMT1_1_01010	FERMT1	-0.398	1.00E-04	0.094
9	BCL2L1_1_11100	BCL2L1	-0.373	1.40E-04	0.096
9	ASL_1_11111	ASL	-0.399	1.40E-04	0.096
11	POLE3_1_11010	POLE3	-0.379	1.40E-04	0.096
12	MYB_1_1111111	MYB	-0.370	3.40E-04	0.213
13	MPP6_1_0110	MPP6	-0.357	4.00E-04	0.225
14	PITX3_1_10111	PITX3	-0.370	4.20E-04	0.225
15	HNF4A_1_10101	HNF4A	-0.360	4.60E-04	0.23
16	DNAJB8_1_011	DNAJB8	-0.362	5.00E-04	0.23
17	PTBP2_1_01001	PTBP2	-0.350	5.20E-04	0.23
18	SOX9_1_11011	SOX9	-0.346	5.80E-04	0.242
19	ZNF573_1_1011	ZNF573	-0.335	6.40E-04	0.253
20	ACTN1_1_0111	ACTN1	-0.343	9.20E-04	0.345
21	ZNF695_1_11111	ZNF695	-0.337	1.06E-03	0.369
22	TNFSF10_1_11011	TNFSF10	-0.340	1.08E-03	0.369
23	PDE3A_1_11111	PDE3A	-0.326	1.14E-03	0.372
24	FUBP1_2_11001	FUBP1	-0.342	1.20E-03	0.372
25	PNLDC1_1_11000	PNLDC1	-0.348	1.24E-03	0.372
26	ODZ1_1_11110	ODZ1	-0.328	1.34E-03	0.384
27	CHI3L2_1_11000	CHI3L2	-0.307	1.38E-03	0.384
28	NRG2_1_01010	NRG2	-0.311	1.44E-03	0.386
29	POMGNT1_1_01111	POMGNT1	-0.323	1.56E-03	0.393
30	ADNP2_1_00011	ADNP2	-0.317	1.62E-03	0.393
31	TRADD_1_0111	TRADD	-0.314	1.64E-03	0.393
32	HDAC4_1_11100	HDAC4	-0.326	1.72E-03	0.393
33	RBM47_1_10010	RBM47	-0.316	1.74E-03	0.393
34	MAPT_1_111	MAPT	-0.333	1.78E-03	0.393
35	HOXA9_1_0111	HOXA9	-0.312	1.90E-03	0.401
36	KIAA0430_1_10100	KIAA0430	-0.313	1.92E-03	0.401
37	AGPAT3_1_0110	AGPAT3	-0.307	2.12E-03	0.417
38	E4F1_1_11110	E4F1	-0.308	2.18E-03	0.417
39	KRAS_1_001111101011	KRAS	-0.336	2.26E-03	0.417
40	CCNE1_1_0111	CCNE1	-0.310	2.30E-03	0.417
41	KPNA5_1_11111	KPNA5	-0.308	2.48E-03	0.417
42	TEAD1_1_10110	TEAD1	-0.293	2.50E-03	0.417
43	FLNB_1_00111	FLNB	-0.299	2.58E-03	0.417
43	FGFR1OP_1_1101	FGFR1OP	-0.298	2.58E-03	0.417
45	WWTR1_1_11111	WWTR1	-0.307	2.62E-03	0.417
46	ADAM21_1_11110	ADAM21	-0.306	2.64E-03	0.417
47	GPR22_1_10110	GPR22	-0.305	2.72E-03	0.417
47	PLXDC2_1_11111	PLXDC2	-0.305	2.72E-03	0.417

47	LMNB2_1_0111	LMNB2	-0.300	2.72E-03	0.417
50	CTNNB1_1_0110	CTNNB1	-0.313	3.04E-03	0.451
51	FOXD2_1_0101	FOXD2	-0.307	3.08E-03	0.451
52	RALGPS2_1_10110	RALGPS2	-0.300	3.14E-03	0.451
53	STK31_1_10001	STK31	-0.310	3.18E-03	0.451
54	CHML_1_1110	CHML	-0.292	3.40E-03	0.463
55	SLC29A3_1_01110	SLC29A3	-0.303	3.50E-03	0.463
56	GYS2_1_11110	GYS2	-0.293	3.52E-03	0.463
57	GBE1_1_0111	GBE1	-0.289	3.66E-03	0.463
58	ITGAV_1_110	ITGAV	-0.284	3.78E-03	0.463
59	CHST2_1_11111	CHST2	-0.285	3.84E-03	0.463
60	ELOVL4_1_01001	ELOVL4	-0.302	3.88E-03	0.463
61	CMKLR1_2_11000	CMKLR1	-0.287	3.94E-03	0.463
62	SAMD4B_1_11111	SAMD4B	-0.295	3.96E-03	0.463
63	HMOX2_1_1011	HMOX2	-0.291	3.98E-03	0.463
64	MICB_1_01111	MICB	-0.293	4.04E-03	0.463
65	CCNB1_1_10111	CCNB1	-0.286	4.16E-03	0.463
66	KCNH4_1_10111	KCNH4	-0.292	4.18E-03	0.463
66	HS3ST5_1_10110	HS3ST5	-0.297	4.18E-03	0.463
68	LGALS13_1_1111	LGALS13	-0.295	4.32E-03	0.463
69	PTGFR_1_11001	PTGFR	-0.285	4.38E-03	0.463
70	NDOR1_1_01001	NDOR1	-0.289	4.42E-03	0.463
71	WT1_1_10001111000	WT1	-0.296	4.44E-03	0.463
71	TMUB1_1_11010	TMUB1	-0.286	4.44E-03	0.463
73	IRX1_1_11111	IRX1	-0.268	4.52E-03	0.465
74	ADARB1_1_01111	ADARB1	-0.282	4.68E-03	0.475
75	KLF16_1_11111	KLF16	-0.277	5.00E-03	0.497

Supplementary Table 6. Table of genes that are essential in samples with focal gene amplification. Top 25 results are shown. Known cancer drivers are highlighted in red.

Rank	ATARiS Solution	Gene	Mean Difference	P-Value	FDR
1	HNF1B_1_11000	HNF1B	-2.81	1.20E-04	0.300
2	OR2T2_1_1001	OR2T2	-1.42	9.00E-04	0.700
3	E2F3_1_11111	E2F3	-1.14	1.22E-03	0.700
4	SRI_1_01011	SRI	-0.94	1.40E-03	0.700
5	GSK3B_1_001111011	GSK3B	-1.34	1.66E-03	0.700
6	ZAP70_1_11101	ZAP70	-0.83	1.80E-03	0.700
7	HOXC13_1_11111	HOXC13	-0.83	2.22E-03	0.700
8	PAX8_1_10011	PAX8	-1.07	2.42E-03	0.700
9	SLC35B3_1_01111	SLC35B3	-1.08	2.52E-03	0.700
10	GH1_1_11011	GH1	-0.89	3.44E-03	0.733
11	CACNG7_1_1111	CACNG7	-1.02	3.68E-03	0.733
12	JUN_1_111110	JUN	-0.86	3.88E-03	0.733
13	SELL_1_01111	SELL	-1.61	4.12E-03	0.733
14	AK5_1_01101	AK5	-1.14	4.18E-03	0.733
15	RPS6KC1_1_11101	RPS6KC1	-0.83	4.40E-03	0.733
16	TFAP2B_1_1111	TFAP2B	-0.97	5.32E-03	0.742
17	GLI1_1_10101	GLI1	-1.09	5.44E-03	0.742
18	TNNI3K_1_11101	TNNI3K	-1.20	6.04E-03	0.742
19	HECTD1_1_01001	HECTD1	-0.93	6.12E-03	0.742
20	RALGPS2_1_10110	RALGPS2	-1.54	7.08E-03	0.742
21	NFE2_1_01101	NFE2	-1.20	7.30E-03	0.742
22	GMFG_1_1110	GMFG	-1.37	7.38E-03	0.742
23	PRTFDC1_1_11110	PRTFDC1	-1.20	7.54E-03	0.742
24	NR1I2_1_11111	NR1I2	-1.04	7.58E-03	0.742
25	SP7_1_11110	SP7	-0.54	7.92E-03	0.742

Supplementary Table 7. Identities of shRNA reagents used.

shRNA	TRC Identifier	NM number	Target (5'-3')
shKRAS-1	TRCN0000033263	NM_033360.2-269s1c1	GACGAATATGATCCAACAATA
shKRAS-2	TRCN0000033260	NM_033360.2-407s1c1	GAGGGCTTTCTTTGTGTATTT
shKRAS	TRCN0000033262	NM_033360.2-509s1c1	CCTATGGTCCTAGTAGGAAAT
shKRAS	TRCN0000033261	NM_033360.2-667s1c1	GATCCGACAATACAGATTGAA
shKRAS	TRCN0000040149	NM_004985.3-641s1c1	GATGCCTTCTATACATTAGTT
shKRAS	TRCN0000040148	NM_004985.3-3896s1c1	CCTCGTTTCTACACAGAGAAA
shKRAS	TRCN0000018337	NM_004985.x-204s1c1	TAGTTGGAGCTGGTGGCGTAG
shKRAS	TRCN0000010369	NM_004985.x-1160s1c1	CAGTTGAGACCTTCTAATTGG
shKRAS	TRCN0000040150	NM_004985.3-570s1c1	CTCAGGACTTAGCAAGAAGTT
shKRAS	TRCN0000040152	NM_004985.3-492s1c1	AGGACTCTGAAGATGTACCTA
shKRAS	TRCN0000040151	NM_004985.3-297s1c1	CTACAGGAAGCAAGTAGTAA
shKRAS	TRCN0000033259	NM_033360.2-4328s1c1	GCAGACGTATATTGTATCATT
shBRAF-1	TRCN0000006293	NM_004333.2-304s1c1	CTATGAAGAATACACCAGCAA
shBRAF-2	TRCN0000006292	NM_004333.2-1538s1c1	CAGCAGTTACAAGCCTTCAAA
shBRAF-3	TRCN0000006291	NM_004333.2-2267s1c1	GCTGGTTTCCAAACAGAGGAT
shBRAF-4	TRCN0000006290	NM_004333.2-838s1c1	CCGCTGTCAAACATGTGGTTA
shBRAF-5	TRCN0000006289	NM_004333.2-1106s1c1	GCAGATGAAGATCATCGAAAT
shPIK3CA-1	TRCN0000010407	NM_006218.x-3234s1c1	AATGAAAGCTCACTCTGGATT
shPIK3CA-2	TRCN0000039607	NM_006218.1-2145s1c1	GCTCATTAACTTAACTGACAT
shPIK3CA*	TRCN0000039603	NM_006218.1-3251s1c1	GATTCCACACTGCACTGTTAA
shPIK3CA-3	TRCN0000039604	NM_006218.1-2368s1c1*	CCAGACATCATGTCAGAGTTA
shPIK3CA-4	TRCN0000039606	NM_006218.1-924s1c1	GCCATCTTATTCCAGACGCAT
shPIK3CA-5	TRCN0000039605	NM_006218.1-1057s1c1	CGAGACATTGACAAGATTTAT
shMYC	TRCN0000010391	NM_002467.x-1970s1c1	CAACCTTGGCTGAGTCTTGAG
shMYC	TRCN0000039638	NM_002467.2-1828s1c1	CCATAATGTAAACTGCCTCAA
shMYC	TRCN0000039639	NM_002467.2-1552s1c1	CCCAAGGTAGTTATCCTTAAA
shMYC	TRCN0000039642	NM_002467.2-1377s1c1	CCTGAGACAGATCAGCAACAA
shMYC	TRCN0000039641	NM_002467.2-408s1c1	CAGGAACTATGACCTCGACTA
shMYC	TRCN0000039640	NM_002467.2-1657s1c1	AATGTCAAGAGGCGAACACA
shHNF1B-1	TRCN0000017508	NM_000458.1-2162s1c1	CCGTACTGTCTATGTTGTGAT
shHNF1B-2	TRCN0000017509	NM_000458.1-734s1c1	CCGACAATTCAACCAGACAGT
shHNF1B-3	TRCN0000017510	NM_000458.1-751s1c1	GCAAATCTTGTACCAGGCCTA
shHNF1B-4	TRCN0000017511	NM_000458.1-800s1c1	CCGACAATTCAACCAGACAGT
shHNF1B-5	TRCN0000017512	NM_000458.1-923s1c	CAGTCCAGAGTTCTGGAAATA
shGFP	TRCN0000072181	clonetechGfp_437s1c1	ACAACAGCCACAACGTCTATA
shLacZ	TRCN0000072231	lacZ_1650s1c1	CGCTAAATACTGGCAGGCGTT

*No data. Virus obtained from the RNAi platform for this shRNA could not infect cells.

Supplementary Methods

Analysis for amplified and essential genes

To derive gene level copy number from the segmented marker data, we used hg-18 to determine gene footprint for available cell lines in the Cell Line Encyclopedia (CCLE; http://broadinstitute.org/ccle), and assigned the minimum marker value as the gene level copy number. The observed pattern of copy number alterations across the genome is analyzed into underlying copy number events using ziggurat deconstruction (Mermel et al. 2011), a maximum likelihood algorithm that uses an empirical probabilistic model of copy number events based on their length and amplitude. Events are then categorized as "broad" or "focal" based on their length relative to their respective chromosome arm, with broad events defined as having arm-relative length greater than 0.95. As broad events are less likely to be related to oncogenic potential of a particular gene (Beroukhim et al. 2010), only focal events were used for further analysis. We considered log2 copy ratio of over 0.3 to be focally amplified. For each gene with at least 6 focally amplified samples in the Achilles RNAi dataset, mean difference of the corresponding gene's ATARiS phenotype values between amplified and non-amplified samples was calculated. We looked for genes that had preferentially lower phenotype values in the context of amplification, and estimated *p*-values from an empirically-derived null distribution by permuting sample labels.

References

Beroukhim R, Mermel CH, Porter D, Wei G, Raychaudhuri S, Donovan J, Barretina J, Boehm JS, Dobson J, Urashima M, et al. 2010. The landscape of somatic copy-number alteration across human cancers. *Nature* **463**: 899–905.

Mermel CH, Schumacher SE, Hill B, Meyerson ML, Beroukhim R, and Getz G. 2011. GISTIC2.0 facilitates sensitive and confident localization of the targets of focal somatic copy-number alteration in human cancers. *Genome Biology* **12**: R41.